Available online at www.sciencedirect.com
SCIENCE DIRECT
Journal of Power Sources 158 (2006) 583–590
JOURNAL OF POWER SOURCES
www.elsevier.com/locate/jpowsour

$LiNi_{0.5}Mn_{1.5}O_4$ thick-film electrodes prepared by electrophoretic deposition for use in high voltage lithium-ion batteries

A. Caballero [a], L. Hernán [a], M. Melero [a], J. Morales [a,*], R. Moreno [b], B. Ferrari [b]

[a] *Departamento de Química Inorgánica e Ingeniería Química, Edificio Marie Curie, Campus de Rabanales, Universidad de Córdoba, 14071 Córdoba, Spain*

[b] *Instituto de Cerámica y Vidrio (CSIC), Campus UAM, 28049 Cantoblanco, Madrid, Spain*

Received 4 July 2005; received in revised form 16 September 2005; accepted 19 September 2005
Available online 2 November 2005

Abstract

Highly homogeneous coatings several microns in thickness were prepared by electrophoretic deposition (EPD) from suspensions of a well-crystallized spinel of nominal composition $LiNi_{0.5}Mn_{1.5}O_4$ mixed with 10% carbon black. The best dispersing conditions were found to be those provided by acetone containing citric acid and polyethyleneimine as dispersing agents; this combination resulted in increased mobility of particles and improved adherence to the substrate. These experimental conditions favored deposition of the smallest particles, thereby increasing coating uniformity. The as-prepared coatings were used as electrodes in lithium cells and found to provide virtually no electrochemical response owing to the lack of interparticle connectivity. This problem was easily overcome by compressing the coatings. Thus, coatings compressed at 517 MPa resulted in cell performance on a par with that of the cell made from the bulk spinel. Moreover, their small particle size facilitates lithium-ion diffusion and the deposits exhibit good rate capabilities and coulombic efficiencies.

Keywords: Electrophoretic deposition; Lithium–nickel–manganese spinel; Lithium batteries

1. Introduction

The increasing tendency to the miniaturization of a variety of portable microelectronic devices involves the necessity of using power sources of reduced size. This challenge can be accomplished by the rechargeable lithium batteries by fabricating their components, electrodes and electrolyte, in the form of films. In recent years, numerous methods have been repeatedly used for the preparation of thin film electrodes from sophisticated and expensive methods, like chemical vapor deposition [1], rf magnetron sputtering [2] and pulsed laser deposition [3], to low cost methods such as spin coating [4], spray [5] and electrospray deposition [6] or electrodeposition [7]. Most of these methods have been applied to the well-known compounds $LiMn_2O_4$ and $LiCoO_2$.

The EPD process is a powerful method for preparing films and coatings [8,9]. The method has been successfully used to obtain various functional materials such as display phosphors [10] or ionic and mixed conductors for fuel cells [11]. In this method an electric field is applied between two electrodes immersed in a low concentrated suspension (usually lower than 5 wt.%), where the charged particles move in response to the electric field. The oriented motion of the charged particles towards the electrode of the opposite sign results in their deposition onto the electrode surface. Compared to press processes, EPD has the general advantages of traditional colloidal cast processes (slip casting, tape casting or gel casting): the resulting materials exhibit a high reliability and microstructural homogeneity. In addition, EPD saves substantial powder during shaping. Because film density does not critically depend on the suspension solid loading in EPD, it allows the preparation of suspensions with a lower solid loading than those required to cast films with a similar density (e.g. by tape casting, spin or spray coating). This avoids the rheological restrictions of most colloidal processes and simplifies suspension conditioning. Also, this method has excellent additional advantages for shaping ternary or binary oxides the most important being that the film thickness and stoichiometry may be easily controlled and that none of the sophisticated equipment

* Corresponding author.
E-mail address: iq1mopaj@uco.es (J. Morales).

0378-7753/$ – see front matter © 2005 Elsevier B.V. All rights reserved.
doi:10.1016/j.jpowsour.2005.09.018

by other coating techniques (e.g. chemical vapor deposition, rf magnetron sputtering, pulsed laser deposition) is needed. Moreover, the EPD method has the ability to simultaneously deposit various materials participating in the pristine suspension. This method has been recently applied with success to the preparation of the positive electrode of lithium batteries using $LiCoO_2$ and $LiMn_2O_4$ as active material [12].

A new family of compounds consisting on Li–Ni–Mn spinels are now in focus because their interesting capabilities. The $LiNi_{0.5}Mn_{1.5}O_4$ spinel is capable of supplying 5 V against the lithium electrode and is representative for a new generation of high voltage lithium rechargeable batteries. This work reports the preparation and characterization of thick-film electrodes made from the $LiNi_{0.5}Mn_{1.5}O_4$ spinel by electrophoretic deposition, focusing processing steps such as the formulation of the EPD kinetics in order to improve the reliability of the process.

2. Experimental

The spinel of nominal composition $LiNi_{0.5}Mn_{1.5}O_4$ (hereafter named LNMO) was prepared from appropriate amounts of Li_2CO_3, $Mn(Ac)_3{\cdot}2H_2O$ and $Ni(Ac)_2{\cdot}4H_2O$ (Ac, acetate) (all supplied by Merck, Germany), using a conventional ceramic method. The starting materials were thoroughly mixed and heated in the air at 800 °C for 6 h. Samples were reground in a mortar and annealed at 800 °C for 24 h. Their lithium content was determined by atomic absorption spectroscopy and their Mn/Ni ratio from energy-dispersive X-ray analysis (EDX) measurements. The average oxidation state of Mn was determined by conventional redox titration [13], and the carbon content of the deposits by using an elemental analyzer (Euro Vector EA-3010, It).

Particle size and shape were analyzed by SEM (Jeol 6400 scanning electron microscope, Japan). Particle size distributions were determined with a laser analyzer (Mastersizers S, Malvern, UK), and surface areas by one point N_2 adsorption (Monosorb, Quantachrome, USA). X-ray diffraction (XRD) patterns were recorded on a Siemens D5000 X-ray diffractometer using Cu Kα radiation and a graphite monochromator for the diffracted beam. The scanning conditions were 15–90° (2θ), a 0.03° step size and 12 s per step.

Spinel coatings were shaped by EPD on graphite, aluminum and stainless steel substrates. Low concentrated suspensions of the spinel powders (2–6.1 g l^{-1}) were prepared in organic solvents to avoid powder–water interactions. Suspensions with a 90/10 (w/w) LNMO/carbon black composition were also prepared. Acetone and ethanol were tested as solvents. Citric acid and polyethyleneimine (PEI) were added as dispersing agents; the former acted as an anionic short-chain surfactant and the latter a cationic surfactant of medium molecular weight. Suspensions were prepared by using both dispersants in ethanol, which resulted in positively charged LNMO particle surfaces. The suspensions in acetone were dispersed the citric acid only owing to the increased basicity. All suspensions were prepared by ultrasonic mixing, using a 400 W sonication probe (IKA U400S, Germany) for 2 min, and subsequent homogenization by mechanical stirring for 30 min. The deposited suspensions were refrigerated during mixing and homogenizing to avoid evaporation of the solvent.

EPD was performed under potentiostatic conditions, using a High Voltage Power Source (Labconco, Mod. 433–3250, USA). Current densities ranging from 0.15 to 4 mA cm^{-2} were applied over periods of up to 10 min. The deposition substrates were discs 1.2 cm in diameter anchored to a graphite working electrode with a 1.2 cm × 1.2 cm area, which ensured that deposition occurred on a single substrate side. The counter electrode was a 1.2 cm × 1.2 cm piece of graphite foil. The working electrode and the counter electrode were anchored to a lift, and placed 2 cm apart. After EPD, samples were withdrawn at a constant rate of 7.5 mm s^{-1} and drying at room temperature was maintained for 5 h. The mass of each deposit was determined by gravimetry.

Two different methods were used to shape the LNMO electrodes. First, pellets 7 mm in diameter were prepared by pressing the active material with carbon black (90:10, w/w) in a stainless steel grid under a pressure of 258 MPa. On the other hand, some of the coatings obtained by EPD were pressed at 295 and 517 MPa prior to insertion into the cell. Electrochemical measurements were made with two-electrode Swagelock-type cells, using Li (supplied by Strem) as anode and a piece of Whatman paper as a spacer. The electrolyte, supplied by Merck, was 1 M anhydrous LiPF6 in a 1:1 mixture of ethylene carbonate and dimethyl carbonate. Cells were assembled in an M-Braun glove-box. Cyclic voltammetry was performed with a Solartron 1286 Electrochemical Interface controlled via the CorrWare and CorrView software packages as run on a PC PentiumII computer. Curves were recorded at a scan rate of 50 μV s^{-1}. Cycling tests were performed on a McPile II (Biologic) potentiostat–galvanostat system under a galvanostatic regime.

3. Results and discussion

3.1. LNMO powder characterization

The XRD pattern for the calcined precursors is shown in Fig. 1a. The strongest lines can be indexed in the spinel structure (space group *Fd*3*m*) and the unit cell dimension obtained, $a = 8.188$ Å, is consistent with those reported for spinels of similar composition [14]. All these peaks are very sharp, which suggests that the sample is highly crystalline. The pattern also exhibits some small peaks at 37.91, 43.86 and 63.5 2θ the spacings of which can be ascribed to NiO or $Li_xNi_{1-x}O$ impurities. This is a common feature when the Ni content (y) in the $LiNi_yMn_{2-y}O_4$ spinel exceeds 0.2% [15]. Under these conditions, substitution of Mn by Ni is difficult and the presence of NiO-like impurities is observed even after repeated calcination. On the assumption of the presence of NiO impurities, the composition of the spinel was calculated by Rietveld refinement of the XRD data [16], using the GSAS software suite [17]. The values obtained for the spinel and NiO phases were 95 and 5%, respectively. Therefore, most Ni is present in the spinel structure and the NiO is only a minor phase.

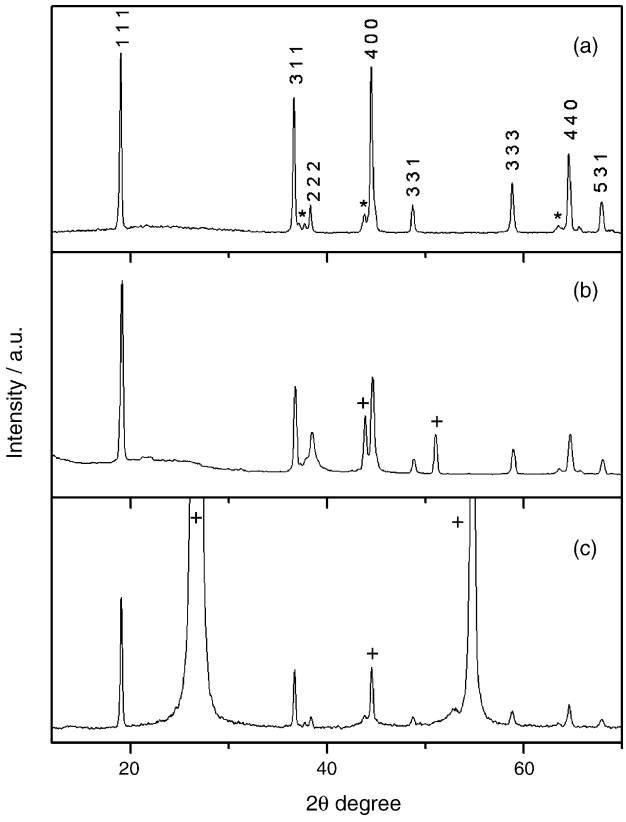

Fig. 1. XRD patterns for (a) the pristine compound and (b and c) EPD deposits on stainless steel and graphite, respectively; applied voltage 100 V. (*) Impurity peaks; (+) substrate.

The results of the chemical analysis are shown in Table 1. The average oxidation state obtained was slightly less than 4; this suggests the presence of Mn^{3+}, which was confirmed by the electrochemical determinations as shown below. These data, together with the composition derived from the XRD pattern, suggest that the spinel possesses a small deficiency in Ni with respect to the ideal formula $LiNi_{0.5}Mn_{1.5}O_4$.

Fig. 2a shows a characteristic SEM micrograph for the spinel powders, as well as the experimentally determined particle size distribution (Fig. 2b). The distribution is of the bimodal type and the average particle size ca. 3 μm. The crystal shape reflects the spinel structure: a high proportion of octahedral or *pseudo*-polyhedral forms with well-defined edges and faces. The micrometric particle size and their smooth surface result in a small specific surface area (only 1.3 $m^2\ g^{-1}$). A low proportion of submicronic particles less well-defined in shape corresponding to either spinel particles of poorer crystallinity and/or the impurity phase was also obtained.

Table 1
Average oxidation state, Mn/Ni and Li/Mn + M ratios and composition of the Li–Ni–Mn spinel

Mn^{n+}	3.87
Mn/N	3.87
Li/Mn + Ni	0.51
Nominal formula	$Li_{1.02}Ni_{0.41}Mn_{1.59}O_4$

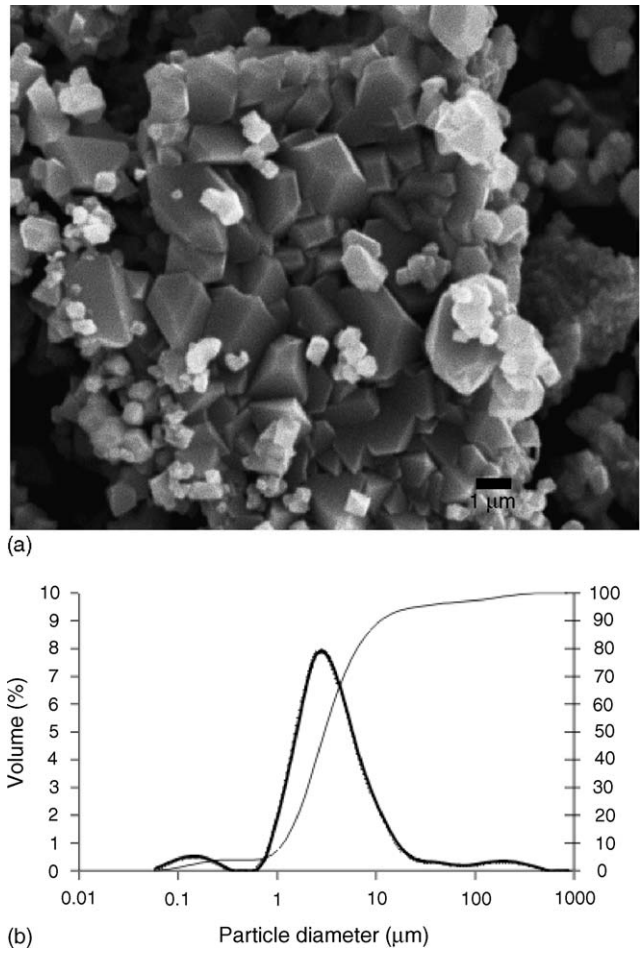

Fig. 2. (a) SEM image and (b) particle size distribution of the pristine compound.

3.2. EPD performance

The suspensions for the EPD experiments were prepared in ethanol and acetone, using PEI and citric acid as dispersants. Table 2 summarizes their characteristics and the processing conditions of the EDP tests. Suspensions in EtOH with solids loadings of 2 and 4.4 $g\ l^{-1}$ were dispersed with 0.4 wt.% PEI and 10^{-2}N citric acid, respectively. The suspensions were stable; however, the deposits obtained at high voltages (up to 250 and 600 V, respectively) were heterogeneous and exhibited poor adherence to the graphite or stainless steel substrates.

The suspensions prepared in acetone were more stable. Homogeneous, strongly adhered coatings (up to 12.8 $mg\ cm^{-2}$) on graphite substrates were obtained by applying 180 V for 1–5 min. However, the deposits on stainless steel and aluminum exhibited poor adherence. Homogeneous, heavier spinel films were deposited on stainless steel and aluminum when citric acid was added to the suspension. However, the suspension conductivity increased with increasing citric acid concentration (from 3.2 $\mu S\ cm^{-1}$ (24 °C) at pH 4 to 8.3 $\mu S\ cm^{-1}$ (24 °C) at pH 2), i.e. both the surface charge of the particles and the ionic concentration of the solution increased and the electrophoretic rate decreased, at a given voltage (100 V) [18]. A lower concentration of citric acid (1.4×10^{-3}N) was thus preferred.

Table 2
EPD conditions used to obtain the LNMO coatings

Medium	Solids ($g\,l^{-1}$)	Deflocculant	Particle charge	Electric conditions			Substrate	Deposition ($mg\,cm^{-2}$)
				V (V)	i ($mA\,cm^{-2}$)	t (min)		
EtOH	4.4	0.4 wt.% PEI	[+]	<250	<3.4	<5	Graphite	Heterogeneous
							S. steel	Heterogeneous
	2	10^{-2}N Citric acid		<600	<6	<5	Graphite	Heterogeneous
							S. steel	Heterogeneous
Acetone	6.1	–	[−]	180	0.5	1–5	Graphite	0.8–12.8[a]
				180	0.5	1–5	S. steel	No deposit
	2	10^{-2}N Citric acid		100	0.5	5	Graphite	Homogeneous
				100	0.5	5	S. steel	4.4
	2	1.4×10^{-3}N Citric acid		100	1	1–10	Graphite	Homogeneous
				100	1	1–10	S. steel	0.8–10.5[a]
				100	1	1–10	Aluminum	1–2.5

[a] Coatings tested in lithium cells.

Fig. 1b shows the XRD pattern for the coating obtained by EPD on stainless steel; as can be seen, it exhibits the same diffraction peaks as the pristine powder of Fig. 1a. The unit cell parameter, 8.191 Å, suggests that any structural change in the spinel during deposition is negligible. Weak diffraction peaks for the substrate were also detected the origin of which may be X-ray scattering on the edge of the substrate. Unfortunately, the presence of these peaks precluded determining the composition as they overlapped with some reflections of NiO. The use of Al and graphite as substrates failed to solve the problem (Fig. 1c) and quantifying the impurity content was impossible. Nevertheless, the fact that the relative intensity of the peaks was preserved suggests that the coating composition is comparable to that of the pristine compound. Moreover, the weakness of the substrate reflection peaks also reflects the high uniformity of the coating. This was later confirmed by the SEM findings.

In order to improve the electrical properties of the coating, LNMO was mixed with carbon black as conducting material. Suspensions of LNMO and carbon black were prepared separately in acetone, using a 1.4×10^{-3}N citric acid solution. Once homogenized both suspensions were mixed in a LNMO/carbon black ratio of 90/10 (w/w). Apparently homogeneous dry coatings were obtained for mixtures deposited on stainless steel or aluminum upon application of 100–200 V for up to 6 min. The carbon content measured, 9.44 wt.%, was similar to that of the initial suspension, which confirms that both components deposited simultaneously.

Fig. 3 shows variation of the mass per unit area as a function of the deposition time for dry deposits obtained from LNMO suspensions stabilized with 1.4×10^{-3}N citric acid by using stainless steel or aluminum as substrates. A voltage of 100 V was applied in both cases. The EPD kinetic results for the LNMO/carbon black mixture at voltages of 100 and 200 V, as obtained for aluminum electrodes as substrates are also shown for comparison.

The growth rate of LNMO deposits is largely dependent on the nature of substrate. When using stainless steel, the deposited mass increases linearly with increasing deposition time, which allows reliable control of the kinetics. Consecutive EPD tests were performed until the concentration of particles in the suspension was reduced by 40 wt.%, after which the linear growing kinetics maintained and no change in suspension conductivity was detected. Therefore, citric acid not only plays a key role in stabilizing particle surfaces by adsorption, but also is a major source of ions and hence responsible for preserving the suspension conductivity. On the other hand, with aluminum as substrate, the mass per unit area deviates from linearity after short deposition times (viz. 3 min), thus hindering control of the deposition thickness. The starting suspensions and the EPD conditions were similar, so these results show that the substrate material itself plays a critical role in the deposit formation that is beyond the scope of this work. Regarding EPD performance, homogeneous LNMO coatings can indeed be obtained on both steel and aluminum substrates; however, thickness control is easier with stainless steel.

Fig. 4a and b shows a general view and a detail of the surface of a 100% LNMO coated aluminum substrate. The size distribution of LNMO particles in the coating is similar to that of the starting powder shown in Fig. 2a; the edges and faces of the *pseudo*-polyhedral forms seem to be more ill-defined, however. Also, the coatings are excessively porous.

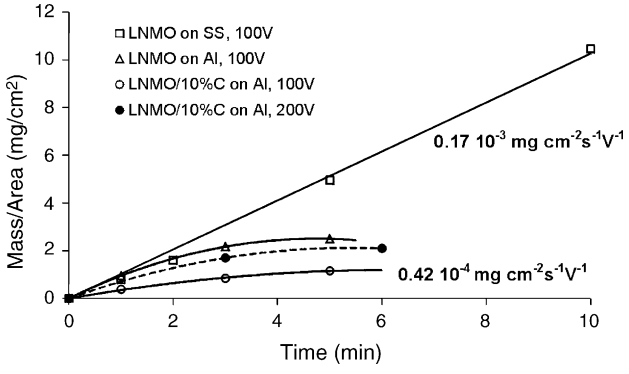

Fig. 3. EPD kinetics of the LNMO deposition on stainless steel and aluminum substrates by applying 100 V, and the 90/10 (w/w) LNMO/carbon black deposition on aluminum substrates by applying 100 and 200 V.

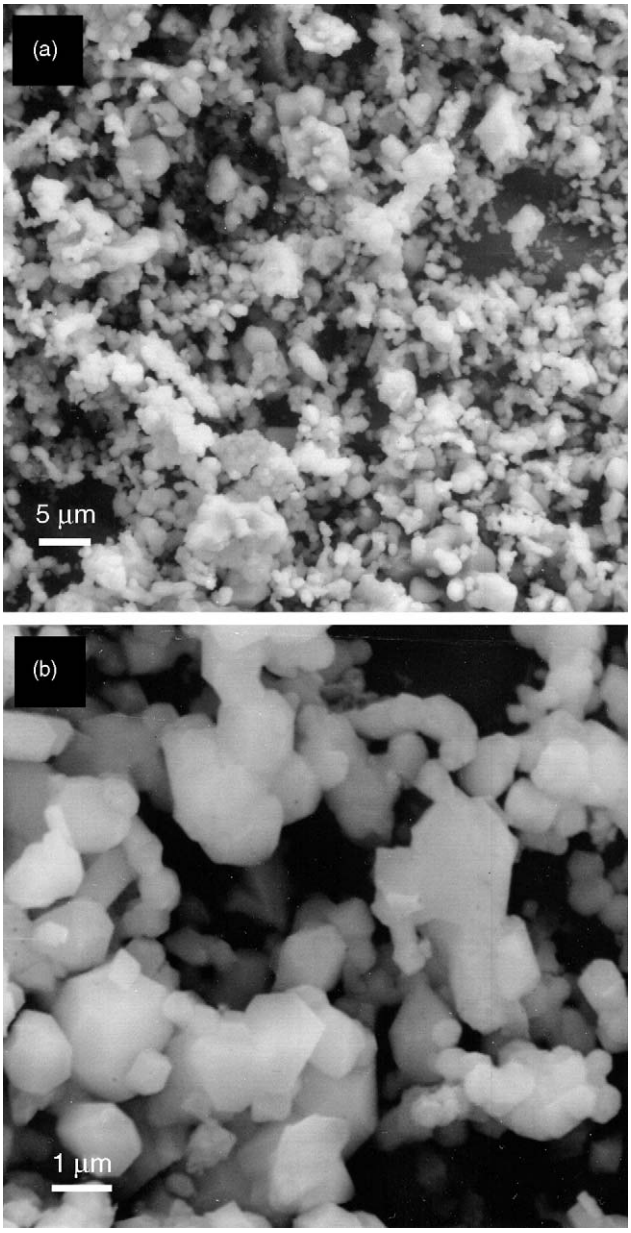

Fig. 4. (a) General top view of LNMO coating on aluminum. (b) Detail of (a). Film deposited on aluminum by applying 100 V to a suspension of 2 g l^{-1} in 1.4×10^{-3}N citric acid.

The growing kinetics for mixtures of LNMO/carbon black deposited on aluminum substrates is even slower (Fig. 3). Thus, the deposition rate over the first 5 min was $\sim 0.42 \times 10^{-4}$ mg cm^{-2} s^{-1} V^{-1}, as compared to $\sim 0.17 \times 10^{-3}$ mg cm^{-2} s^{-1} V^{-1} for LNMO without carbon black. The incorporation of carbon black hinders the stabilization of the suspension and decreases electrophoretic mobility. Various binders commonly used in ceramic processing (CMC, PEG) were tested with a view to improving adhesion of particles in the deposit that proved ineffective, however. Some increase in mass was obtained by raising the applied voltage to 200 V, where the deposited mass per unit area was twice that obtained by using 100 V for the same time.

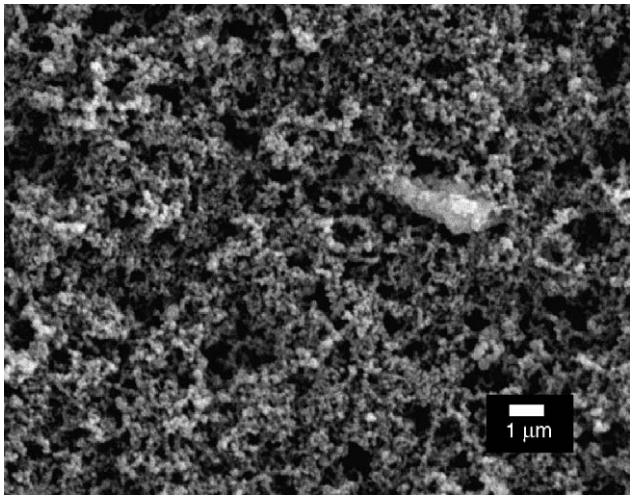

Fig. 5. Top view of a LNMO/carbon black coating. The experimental conditions were similar to those used for the deposit of Fig. 4 except for the substrate, which was stainless steel.

Fig. 5 shows a SEM image of the surface of a LNMO/carbon black coating. A porous deposit was obtained the microstructure of which reveals that the morphology of the grains differs somewhat from that of the starting powder. Particle size is smaller (below 0.5 μm) and more homogeneously distributed. Also, the polyhedral morphology is lost and particle contours are more irregular and ill-defined. Differences in particle size between the pristine and deposited samples were also reported in Ref. [12]. The differences can be ascribed to two factors. Thus, the decreased mobility of the suspension containing carbon black facilitates the migration and further deposition of the fine fraction of powder, which is consistent with the low deposition rates measured. In order to stabilize the mixture, citric acid must interact with both LNMO and carbon clack particles. However, because carbon black provides such a large surface area, the concentration of citric acid is insufficient to coat the particles. Furthermore, the acid conditions used in this work can cause some dissolution at particle surfaces, thus softening the starting *pseudo*-polyhedral morphology.

3.3. Electrochemical characterization

The electrochemical response of the deposits was initially monitored by cyclic voltammetry (CV). Fig. 6a shows the CV curve for the LMNO coating obtained by deposition onto graphite substrate using acetone without a stabilizer. No peaks related with the spinel were observed either in the anodic or cathodic scan; this suggests the absence of extraction or insertion of Li ions typical of the electrochemical behavior of this spinel in lithium cells. The broad peak at 4.95 V in the anodic scan can be assigned to intercalation of PF_6^- anions into the graphite structure as recently reported by Seel and Dahn [19]. Thus, this layered structure is unsuitable for used as a substrate for the active material in high voltage lithium cells. Surprisingly, the coatings obtained on stainless steel failed to provide the expected electrochemical response of the spinel: no peaks were detected in the CV curve (Fig. 6b) for the LNMO spinel

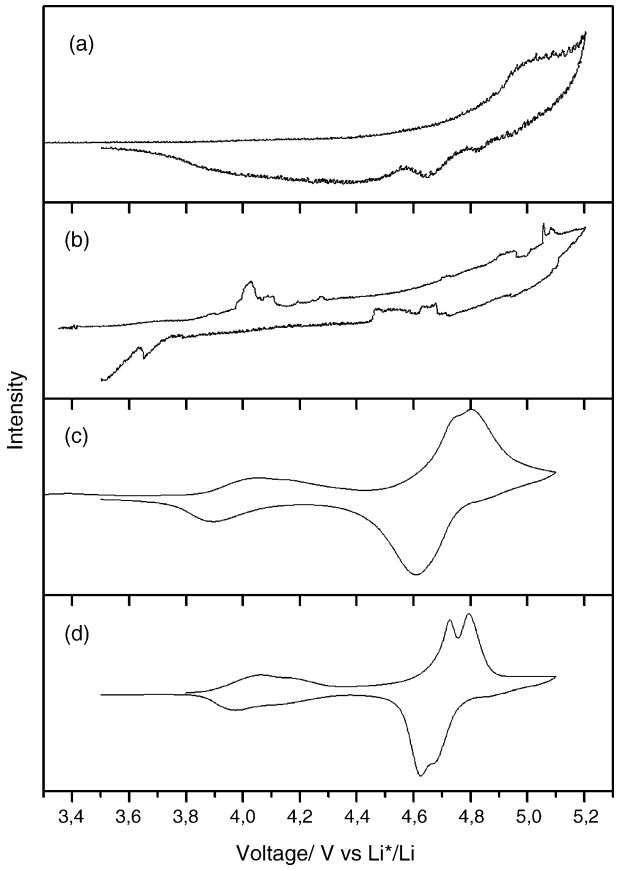

Fig. 6. Cyclic voltammograms for EPD films on various substrates: (a) graphite, (b and c) stainless steel and (d) aluminum. Coatings (c and d) were pressed at 517 MPa. The last contained 10 wt.% carbon black.

or that mixed with 10 wt.% carbon black. Nor did the CV curves for the deposits obtained by adding a binder such as PTFE to the suspension showed any signs of electrochemical reaction.

The results of the electrochemical tests suggest that the poor electrochemical behavior observed is related to a high impedance that is probably a result of reduced connectivity between particles and also perhaps, between particles and the substrate, despite the apparent good adherence exhibited by the deposits. In order to increase contact between particles and with the substrate, the deposit was further compacted by axial pressing. Fig. 6c shows the CV curve for an LMNO deposit on stainless steel pressed at 517 MPa. Under these conditions, the electrochemical response of the electrode was as expected for a Li–Ni–Mn spinel. The signals for the deposit prepared on aluminum from a suspension containing 10 wt.% carbon black were better resolved, which suggests improved conductivity in the electrode (Fig. 6d). For this reason, all cycling tests shown below were performed using deposits prepared on aluminum as substrate. Our results depart from those of Kanamura et al. [12], who found an acceptable electrochemical behavior for $LiCoO_2$ and $LiMn_2O_4$ electrodes obtained by EPD in the absence of pressure—no reference to electrode compression was made. One other minor discrepancy is the absence of electrochemical response from carbon-free deposits.

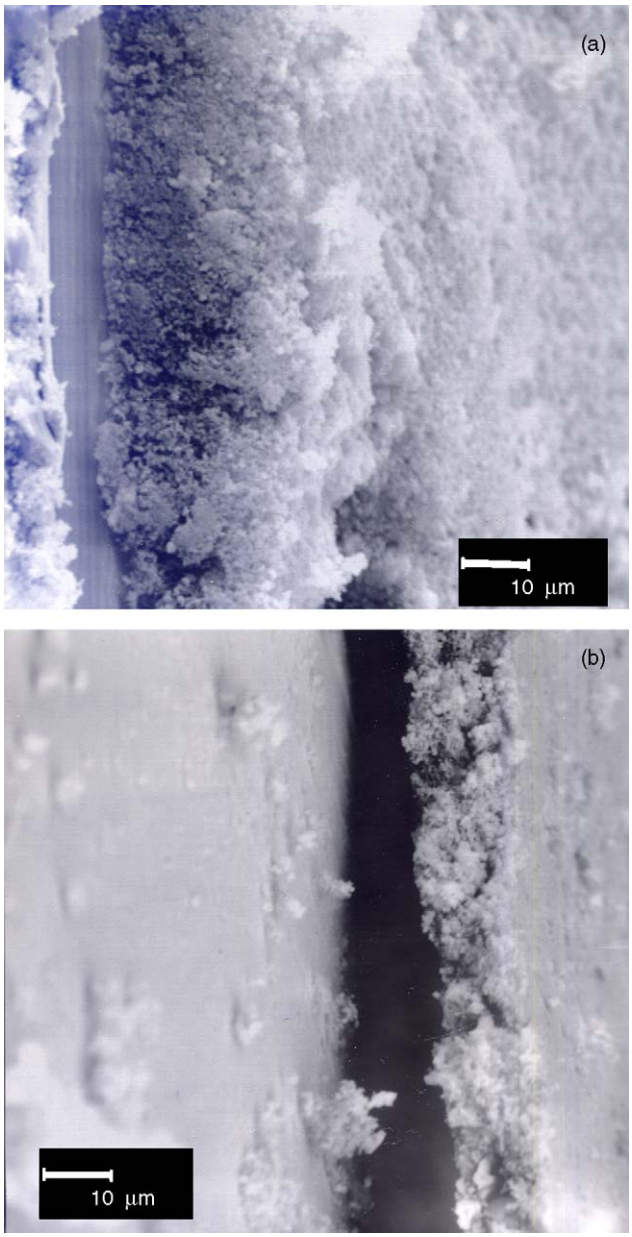

Fig. 7. Cross-sectional view of the coating deposited before (a) and after pressing at 517 MPa (b).

Fig. 7a shows a SEM image of the cross-section of an LNMO/carbon black coating before axial pressing. A porous deposit with uniform thickness of ~40 μm and well adhered to the substrate surface was obtained. Fig. 7b is a cross-section image of the deposit after pressing at 517 MPa. The pressed electrode exhibited a higher density and more uniform compaction, and resulted in a markedly reduced coating thickness. The electrochemical response in the 3.9–4.3 V region due to the oxidation of Mn(III) to Mn(IV) was barely detected; this is consistent with the high oxidation state of Mn in the spinel (see Table 1). Electrochemical activity was observed mainly in the 4.7–5.0 V region, where a double peak associated to the $Ni^{2+} \rightarrow Ni^{4+}$ process, the mechanism of which involves two cubic/cubic two-phase reactions [20], was obtained. Also based on spectroscopic results [21,22] the oxidation of Ni^{2+} to Ni^{4+} takes place via the follow-

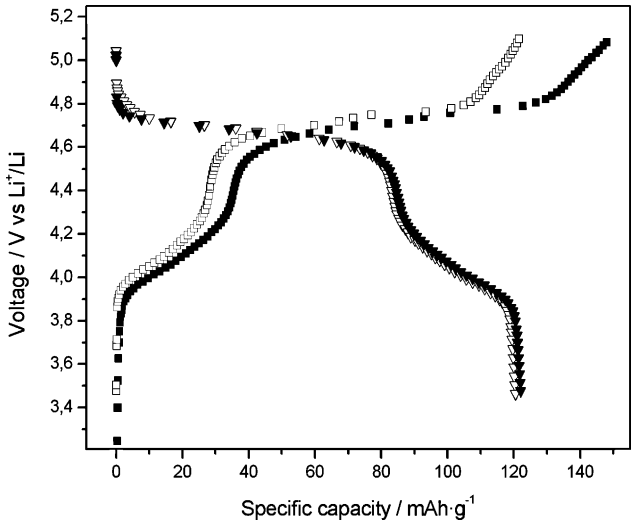

Fig. 8. Charge–discharge curves for the EP deposits cycled over the voltage range 3.5–5.0 V; (■) first charge and (□) second charge; (▼) first discharge and (▽) second discharge. Galvanostic curves recorded at a *C*/6 rate.

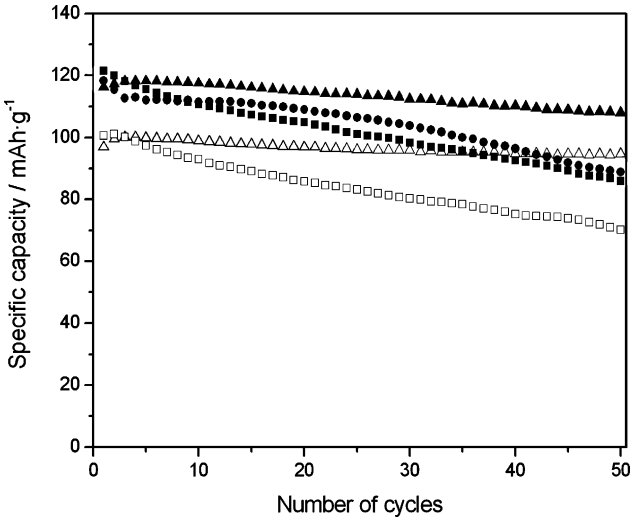

Fig. 9. Variation of the specific discharge capacity of Li/Li–Ni–Mn–O cells cycled over the voltage range 3.5–5.0 V. Bulk material (●), coatings pressed at 295 MPa (□) and at 517 MPa (■) (charge/discharge rate *C*/6). Coatings pressed at 517 MPa (▲) *C*/4; (△) 1*C*.

ing reactions involving Ni^{3+}:

$$Li[Ni(II)_{0.5}Mn(IV)_{1.5}]O_4 \rightarrow Li_{0.5}[Ni(III)_{0.5}Mn(IV)_{1.5}]O_4 + 0.5Li^+ + 0.5e^-$$

$$\rightarrow [Ni(IV)_{0.5}Mn(IV)_{1.5}]O_4 + 0.5Li^+ + 0.5e^-$$

These processes are reversible and take place at somewhat lower voltages.

Cycling performance was examined in cells made from the electrodes prepared using the deposits obtained with carbon black on aluminum. Also, a reference cell was made from an electrode formed merely by pressing the pristine compound mixed with 10% of carbon black on a stainless steel grid. Fig. 8 shows the first two charge/discharge curves for the electrode obtained from EP deposits. Consistent with the CV profiles, the main electrochemical activity of the Ni spinels was seen above 4.5 V. Below such a voltage, a small plateau with a calculated capacity of ca. 30 mAh g^{-1} was observed, which is consistent with the Mn^{3+} content obtained from the composition data in Table 1. Moreover, the capacity of the first charge considerably exceeds that of the first discharge. This overcharge has been commonly reported to occur above 4.9 V and has been ascribed to the release of oxygen from the spinel lattice [23]. The second cycle tends to equilibrate the charge and discharge capacity values, once the spinel lattice has been stabilized. Fig. 9 shows the discharge capacity delivered by the cells on prolonged cycling. Data were recorded at a charge/discharge rate of *C*/6 (*C* being the theoretical capacity delivered in 1 h) and over the voltage window 3.5–5.1 V. The influence of pressure – and hence of the degree of compaction of the deposits formed by EPD – is clearly apparent from the capacity delivered by the electrode at 295 and 517 MPa (100 and 122 mAh g^{-1}, respectively). The latter value is similar to that obtained for the reference cell (119 mAh g^{-1}). Although the discharge capacity of the two electrodes decreased with cycling, the capacity loss was somewhat more pronounced for the cell made from the EP deposit.

The rate capabilities of these electrodes were examined at three different charge/discharge rates, namely *C*/6, the results are discussed above, *C*/4 and 1*C*. The variation of capacity as a function of the number of cycles at the two latter values is also shown in Fig. 9. Although the capacity delivered by the cell at *C*/4 was initially slightly lower than that measured at *C*/6, it surpassed it after the fifth cycle, beyond which capacity retention clearly improved. This trend was also observed at 1*C* even though a decreased discharge capacity value was expected. One plausible explanation for the improved capacity retention at increased the charge/discharge rates is related to particle size in the deposits. As shown above, the particle fraction that deposited was that of the smallest size (below 500 nm). One of the advantages of materials with a small particle size in lithium cells is the good rate performance they deliver by virtue of their short diffusion paths for lithium ions. The decrease in capacity on cycling at the lowest discharge rate tested may have been a result of a degradation (dissolution) of the active material by reaction with the electrolyte—the increased reactivity of small particles can facilitate electrolyte decomposition [24]. In fact, the capacity loss on cycling in the cell made from the spinel in the form of pellets, where both submicrometic and micrometric particles were present was somewhat small relative to the cell made from the coating. Degradation was less marked at increased charge/discharge rates and the effect of a decreased particle size prevailed and resulted in improved cell performance. Further work is currently being conducted wit a view to optimizing the EPD parameters for manufacturing coatings with a higher density and interconnectivity between particles on aluminum substrates.

The coulombic efficiency of the electrode made from the deposit on aluminum pressed at 517 MPa is shown in Fig. 10 together with that of the electrode made from the bulk material for comparison. The low values of the first few cycles (below 95%) resulted from the above-described significant overcharge.

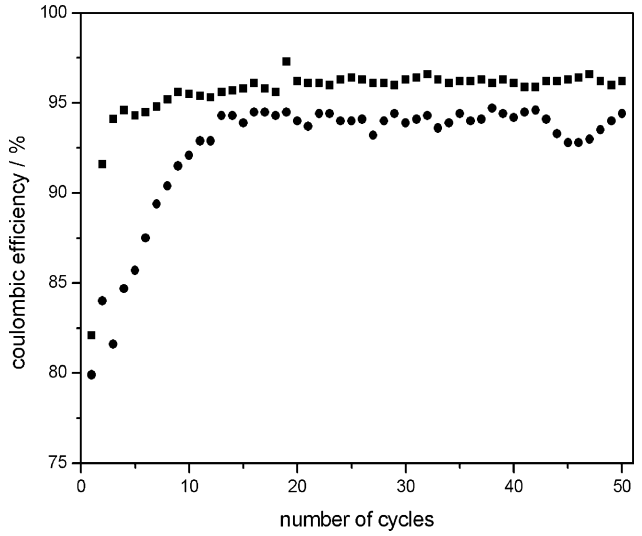

Fig. 10. Variation of the coulombic efficiency of Li/Li–Ni–Mn–O cells as a function of the number of cycles. Bulk material (●), coating pressed at 517 MPa (■) (charge/discharge rate *C*/6).

In subsequent cycles, the coulombic efficiency of the electrode remained at quite high levels (95–97%). The cells made from the bulk spinel required a greater number of cycles to reach an efficiency level around 93% (i.e. somewhat lower than that of the EPD electrode).

4. Conclusions

The electrophoretic deposition method is a suitable low-cost coating tool for the preparation of $LiNi_{0.5}Mn_{1.5}O_4$ electrodes to be used in high voltage lithium batteries once the compactness and density of the coatings are optimized simply by pressing. The coatings obtained at the experimental deposition conditions studied are highly uniform, exhibit good adherence the substrate; also, their thickness can be easily controlled. Both the discharge capacity of the cells made from these coatings and cell performance were similar to those of a cell made from the bulk compound. The small particle size of the deposits favors lithium diffusion by shortening the distance to be travelled by the ions, which improves the rate capabilities of the electrode.

Acknowledgements

This work was supported by Junta de Andalucía (Group FQM-175) and Ministerio de Ciencia y Tecnología (Projects MAT2002-04477-C02-02 and MAT2003-00836).

References

[1] P. Liu, J.G. Zhang, J.A. Turner, C.E. Tracy, D.K. Benson, J. Electrochem. Soc. 146 (1999) 200.
[2] M.M. Thackeray, M.F. Mansuetto, J.B. Bates, J. Power Sources 68 (1997) 153.
[3] Y. Wang, Z.W. Fu, Q.Z. Qin, Thin Solid Films 441 (2003) 19.
[4] Y.H. Rho, K. Kanamura, T. Umegaki, J. Electrochem. Soc. 150 (2003) A107.
[5] Y.J. Park, J.G. Kim, M.K. Kim, H.T. Chung, W.S. Um, M.H. Kim, H.G. Kim, J. Power Sources 76 (1998) 41.
[6] A.A. Vanzomeren, E.M. Kelder, J.C.M. Marijnissen, J. Schoonman, J. Aerosol Sci. 25 (1994) 1229.
[7] J. Morales, L. Sánchez, S. Bijani, L. Martínez, M. Gabás, J.R. Ramos-Barrado, Electrochem. Solid-State Lett. 8 (2005) A159.
[8] O. Van der Biest, L. Vandeperre, Ann. Rev. Mater. Sci. 29 (1999) 327.
[9] P. Sarkar, P.S. Nicholson, J. Am. Ceram. Soc. 79 (1996) 1987.
[10] K.Y. Sasaki, J.B. Talbot, Adv. Mater. 11 (1999) 91.
[11] L.C. De Jonghe, C.P. Jacobson, S.J. Visco, Ann. Rev. Mater. Res. 33 (2003) 169.
[12] K. Kanamura, A. Goto, J. Hamagami, T. Umegaki, Electrochem. Solid-State Lett. 3 (2000) 259.
[13] L. Hernán, J. Morales, L. Sánchez, J. Santos, E. Rodríguez Castellón, Solid State Ionics 133 (2000) 179.
[14] P. Strobel, A. Ibarra Palos, M. Anne, F. Le Cras, J. Mater. Chem. 10 (2000) 429.
[15] Y. Ein-Eli, J.T. Vaughey, M.M. Thackeray, S. Mukerjee, X.Q. Yang, J. McBreen, J. Electrochem. Soc. 146 (1999) 908.
[16] H.M. Rietveld, J. Appl. Crystallogr. 2 (1969) 65.
[17] A.C. Larson, R.B. Von Dreele, Los Alamos National Lab., Rep. No. LA-UR-86-748, 1994.
[18] B. Ferrari, R. Moreno, J. Electrochem. Soc. 147 (2000) 2987.
[19] J.A. Seel, J.R. Dahn, J. Electrochem. Soc. 147 (2000) 892.
[20] K. Ariyoshi, Y. Iwakoshi, N. Nakayama, T. Ohzuku, J. Electrochem. Soc. 151 (2004) 296.
[21] K. Amine, H. Tukamoto, H. Yasuda, Y. Fujita, J. Electrochem. Soc. 143 (1996) 1607.
[22] T. Terada, K. Yasaka, F. Nishikawa, T. Konishi, M. Yoshio, I. Nakai, J. Solid State Chem. 156 (2001) 281.
[23] A. Caballero, L. Hernán, M. Melero, J. Morales, M. Angulo, J. Electrochem. Soc. 152 (2005) A6.
[24] G.G. Amatucci, A. Blyr, C. Sigala, P. Alfonse, J.M. Tarascon, Solid State Ionics 104 (1997) 138.